ORNL/CP-98139

CONF-981054--

Room-Temperature Serrated-Flow Behavior in Fe-rich FeAl under Vacancy Supersaturation

K. Yoshimi, M. H. Yoo and S. Hanada*

Metals and Ceramics Division, Oak Ridge National Laboratory
Oak Ridge, TN 37831-6115
*Institute for Materials Research, Tohoku University, Sendai 980-77, Japan

Abstract

In Fe-rich FeAl, serrated plastic-flow behavior has been observed for the first time at room temperature. Serration on the tensile stress-strain curve occurs in single crystals that retained supersaturation of thermal vacancies after fast-cooling from the annealing temperature of 1173 K. In contrast to conventional serrated flow, the serrated flow in FeAl is associated with work hardening, and it becomes more pronounced with increasing Al content from 33 to 44 mol.%. The experimental results are interpreted in terms of the dynamic interaction of $(\bar{1}01)[111]$ superdislocations with the excess thermal vacancies and their clusters, and the successive double cross-slip of screw superdislocations at the moving front of a slip band. The strong dependence on alloy composition and the lack of strain-rate sensitivity are discussed.

DISCLAIMER

DISCLAIMER

Portions of this document may be illegible in electronic image products. Images are produced from the best available original document.

Introduction

In the last decade, many research efforts have been made to investigate the strength of B2 FeAl, such as the excess-vacancy hardening and the yield stress anomaly. A number of the recent papers suggest mechanisms for the yield stress anomaly based on experimental results [1-4], but only a few papers address the question why excess vacancies harden Fe-Al so much. Chang et al. [5] reported that hardness in B2 FeAl has a linear relationship with the square root of the vacancy concentration. This relationship may be interpreted in terms of the solid solution hardening proposed by Fleischer and Hibbard [6] and Friedel [7]. However, Pike et al. [8] concluded that the solution hardening rate by vacancies is higher than that seen in many substitutional solid solutions, and thus there may be an as-yet unrevealed additional mechanism that is involved in the vacancy hardening. In our recent single crystal study at room temperature [9], serrated flow behavior was observed in vacancy-containing Fe-Al. Such a behavior has never been observed at room temperature till now. The analyses of this behavior may give some clues to find the mechanism of the excess-vacancy hardening.

In this paper, the room-temperature serrated-flow behavior observed in vacancy-supersaturated Fe-Al is highlighted. The serrated flow and the excess-vacancy hardening are discussed based on off-stoichiometric effects on defect properties, supersaturated vacancy concentration, work-hardening, and strain-rate sensitivity.

Experimental

Effects of vacancy supersaturation and Al content on room temperature deformation of Fe-Al were investigated by tensile testing of three different single crystals (Fe-33, 41 and 44 mol.%Al). The total interstitial impurities in these alloys were nominally below 22 wt.ppm (C < 18, O < 7, N < 1 and H ≈ 1) The tensile axes of the specimens were close to the $[\bar{1}23]$ direction. All the tensile specimens received a homogenization heat treatment at 1373 K for 48 hs, followed by slow cooling at 0.005 $K \cdot s^{-1}$ to room temperature inside the furnace. Subsequently, these specimens were vacuum-sealed in silica tubes, and re-annealed at 1173 K for 1 h, followed by fast cooling outside the furnace to introduce excess vacancies. Before tensile tests, specimen surfaces were mechanically polished and electropolished in perchloric acid-methanol solution. Tensile tests were conducted using an Instron 8562-type machine in a vacuum better than 2×10^{-3} Pa at room temperature.

Figures 1 and 2 show resolved shear stress - strain curves of the as-homogenized and the fast-cooled three single crystals, respectively. The critical resolved shear stresses (CRSSs) are raised prominently due to excess vacancies. It was noted that all fast-cooled specimens displayed serrations with work-hardening. In Fe-41 and 44Al, this serrated flow behavior continues until the specimens failed. Figure 3 shows highly magnified resolved shear stress - strain curves for the fast-cooled specimens. It is clear that the serrated flow behavior is more pronounced for the higher Al content. Since the excess vacancy concentration is higher for the higher Al content in B2 FeAl when samples receive the same heat treatments [5, 10], the change in these jerky flow characteristics depending on Al content would likely result from the change

n excess vacancy concentration.

The strain-rate sensitivity of flow stress was examined by changing the strain-rates etween 1×10^{-4} and 1×10^{-5} s^{-1}. Figure 4 shows resolved shear stress-strain curves of fast-ooled (a) Fe-41 and (b) 44Al single crystals. Due to the unstable nature of jerky flow, ansients in the flow stress change could not be detected. The serrated flow behavior was ound to be rather insensitive to strain-rate changes.

Discussion

The present paper gives the first experimental evidence of serrated flow behavior in Fe-ich FeAl single crystals at room temperature when large amounts of supersaturation of thermal acancies were retained. In the earlier work [2, 11], serrated plastic flow behavior associated vith the propagation of coarse slip bands was reported in Fe-39Al single crystals at 823 K, vhich is the peak temperature of the yield strength anomaly in this alloy. The results of this earlier work are briefly summarized before discussing the current results.

When Fe-39Al single crystals were deformed in compression along the $[\bar{1}23]$ direction at 823 K, serration on the stress-strain curves was detected in the early stage of work-hardening. The slip-trace analysis on two surfaces indicated that the serrated flow behavior was associated with the heterogeneous formation of slip lines and the propagation of Lüders-like bands, with a [111] slip vector. In the later stage of plastic flow (beyond about 3% strain), when the slip bands covered the whole compression samples, the serration disappeared and work-softening occurred. In the later stage, the active slip vector was identified by TEM to be of the <010>-ype. The slip vector transition from [111] to <010> can be explained by the dislocation decomposition model [12]. A Lüders band propagation is associated with a dislocation avalanche moving once into unyielded material. To explain this behavior, the model related to double cross-slip pinning and to dislocation locking by solute atom atmosphere have been proposed [13, 14]. Dislocation mechanisms responsible for the Lüders-like slip band propagation in B2 FeAl at the peak temperature are thought to be involved with both the cross slip of $(\bar{1}01)[111]$ screw superdislocations into the $(\bar{1}10)$ or $(\bar{2}11)$ plane and the interaction of non-screw dislocations with thermal vacancies at this transition temperature [11].

Dynamic Interaction of Dislocations with Point Defects

At room temperature, the active slip system in tensile specimens along the $[\bar{1}23]$ direction of the single crystals with three Fe-rich compositions (Fe-33, 41 and 44Al) is expected to be $(\bar{1}01)[111]$. Post mortem TEM analyses of the deformed samples reported elsewhere [9] confirmed the active slip system.

As compared to the Fe-39Al compression specimens, the tensile specimens of the three different compositions had received the additional heat treatment of annealing at 1173 K for 1 h, followed by fast cooling down to 300 K. Therefore, a large supersaturation of non-equilibrium thermal vacancies must have existed in each tensile sample prior to deformation. It

is these excess vacancies that are thought to cause jerky flow of $(\bar{1}01)[111]$ superdislocations, discontinuous propagation of slip bands, and consequently the serrated stress-strain curve. The coarse slip band propagation observed in Fe-39Al compression specimens [2, 11] was very much like the conventionally observed Lüders-band phenomenon in association with a single deformation front traveling along a specimen [15]. But, no direct observation of slip band propagation was made in the present work.

The source and multiplication mechanisms of $(\bar{1}01)[111]$ superdislocations for the heterogeneous initiation of slip lines are not understood, but the prismatic dislocation loops resulting from clustering of the quenched-in vacancies have presumably played some role in the generation of mobile dislocations [16]. Once a coarse slip band is formed, to move the front of the slip band into the undeformed matrix requires an additional multiplication mechanism of mobile dislocations. In this case, the successive double cross-slip of screw superdislocations may play an important role in effecting the slip band propagation as in the case of α-brass [14].

The serrated flow behavior observed in FeAl single crystals is distinctly different from the conventional Lüders-band phenomenon in that it occurred always during work hardening and it is rather insensitive to the applied strain rate (see Fig. 4). In the present case, point defects are considered to be immobile at room temperature, and the dynamic interaction of the front of the slip band with the point defects is to be controlled by the mobility of $(\bar{1}01)[111]$ dislocations. The roughness of serrated flow behavior becomes more pronounced with the increase in Al content as shown in Figs. 2 and 3. Therefore, the sensitivity of dislocation and defect properties to the alloy composition is an important factor that may shed light on our mechanistic understanding of the propagative plastic instability of FeAl single crystals.

Effects of Composition on Dislocation and Vacancy Properties

In off-stoichiometric FeAl crystals, constitutional defects of several types must exist, such as anti-site defects and constitutional vacancies. It is unlikely, however, that the observed serrated-flow behavior was influenced by these constitutional defects, because the observed behavior was found to be less pronounced with the deviation to the Fe-rich side further away from the B2 stoichiometry (Figs. 2 and 3).

According to the equilibrium phase diagram [18], the DO_3 structure is stable at room temperature when the Al content is less than 36 mol.%. Although the equilibrium dissociation configurations of a superdislocation in the DO_3 and B2 structures are four-fold and two-fold, respectively, the important dislocation configuration in the present case is the two-fold dissociation for all three alloy compositions. This is because of the fact that in Fe-33Al the long-range DO_3 ordering is decreased by the DO_3 off-stoichiometry, the DO_3-type APB energy is reduced, and thus the leading and trailing superpartial pairs move independently as the B2-type superlattice dislocations [19-21]. At room temperature, the elastic shear anisotropy in FeAl is known to increase with decreasing Al content [22]; i.e., Fe-33Al is elastically more anisotropic than Fe-44Al. If the effect of elastic anisotropy is to increase the effective dislocation width and to decrease the Peierls stress [23], the intrinsic mobility of $(\bar{1}01)[111]$ superdislocations should decrease as the Al content is increased from 33 to 44 mol.%. Furthermore, if the line

ension instability was to contribute directly to the formation of slip bands, the effect of elastic anisotropy seems to be opposite to the compositional dependence of the serrated flow behavior observed in this work.

It is now well established that a very high concentration of thermal vacancies exists in B2 FeAl at elevated temperatures. Table 1 lists the available vacancy parameters of B2 FeAl. Fu et al. [33] determined the formation enthalpies of vacancies and anti-site defects in stoichiometric FeAl using first-principles quantum mechanical calculations based on the local-density-functional theory. The calculated results give the vacancy formation enthalpy of H_V^F = 0.97 eV at Fe sites, the anti-site defect formation enthalpy of 0.95 eV at Al sites, and 1.04 eV at Fe sites. These relatively low energies of defect formation, together with the vacancy binding energy of 0.57 eV [33], suggest a strong possibility of the formation of defect complexes, such as divacancies. Using the data obtained by Würschum et al. [29], which had taken account of divacancy formation, one can obtain the equilibrium concentrations of vacancies and divacancies as functions of temperature as shown in Fig. 5. This result shows that at the annealing temperature of 1173 K the divacancy concentration, $C_{2V} \approx 0.016$, is higher than the monovacancy concentration, $C_V \approx 0.01$. As shown in Table 1, the vacancy migration enthalpy is much larger than the vacancy formation enthalpy. This is one of the unique characteristics of FeAl not seen in ordinary metals and alloys.

Because of such a high vacancy migration enthalpy, defect migration is sluggish even at high temperatures, and thermal vacancies are easily retained upon rapid cooling. As for the composition dependency of vacancy properties, though a large scatter in the available data, the available experimental values in Table 1 seem to show some trends dependent on Al concentration. However, Figs. 1 and 2 show clearly the marked increase in the CRSS of FeAl as the Al content is raised in single crystals, which had retained excess vacancies by rapid cooling from 1173 K. This result is consistent with the hardness data [5, 10]. These experimental results support the contention that the enhanced serrated flow behavior in Fe-44Al at room temperature, as compared to Fe-33Al and Fe-41Al, is due primarily to the higher concentrations of vacancy and its complexes that were retained in the specimen. Much more work is needed to elucidate the effects of composition on defect properties and to develop a micromechanical model for the serrated flow behavior in terms of strain, strain rate, and temperature.

Summary

Serrated flow is observed at room temperature in rapidly-cooled, i.e., excess-vacancy hardened, Fe-rich Fe-Al by tensile deformation. The serrated flow behavior is more pronounced for the higher Al concentration. This trend corresponds to the increase in the CRSS with the increase in excess vacancy concentration as the Al content increase. This is in contrast to the opposite trend of the compositional dependence of the constitutional defect concentrations, APB energy, and the line-tension instability. Therefore, it is concluded that this serrated flow behavior is attributed to the supersaturation of excess thermal vacancies. The serrated-flow behavior observed in Fe-Al is accompanied by work-hardening, and it exhibits

negligible strain-rate sensitivity. These are the unique distinctions from the conventional serrated flow behavior observed in dynamic strain-aging alloys.

Acknowledgments

The authors thank Dr. J. H. Schneibel and Dr. L. M. Pike for reviewing the manuscript. This research was sponsored by the program of Japan Society for the Promotion of Science Postdoctoral Fellowships for Research Abroad, and in part by the Division of Materials Sciences, U.S. Department of Energy, under Contract No. DE-AC05-96OR22464 with Lockheed Martin Energy Research Corp.

References

1. D. G. Morris, *Phil. Mag. A*, **71** (1995), 1281.
2. K. Yoshimi, S. Hanada and M. H. Yoo, *High-Temperature Ordered Intermetallic Alloys VII*, MRS Symposium Proceedings, Vol. 460, ed. C. C. Koch, C. T. Liu, N. S. Stoloff and A. Wanner (Pittsburgh, PA: Materials Research Society, 1996), 313.
3. F. Král, P. Schwander and G. Kostorz, *Acta Mater.*, **45** (1997), 675.
4. E. P. George and I. Baker, *Phil. Mag. A*, **77** (1998), 737.
5. Y. A. Chang, L. M. Pike, C. T. Liu, A. R. Bilbrey and D. S. Stone, *Intermetallics*, **1** (1993), 107.
6. R. L. Fleischer and W. R. Hibbard, Jr., *The Relation between the Structure and Mechanical Properties of Metals*, (London: H. M. S. O., 1963), 605.
7. J. Friedel, *Microscopy and Strength of Crystals*, ed. G. Thomas and J. Washburn (New York, NY: Interscience, 1963), 605.
8. L. M. Pike, Y. A. Chang and C. T. Liu, *Acta Mater.*, **45** (1997), 3709.
9. K. Yoshimi, Y. Saeki, M. H. Yoo and S. Hanada, *Mater. Sci. Eng. A*, (1998), to be published.
10. P. Nagpal and I. Baker, *Metall. Trans. A*, **21** (1990), 2281.
11. K. Yoshimi, M. H. Yoo and S. Hanada, *Acta Mater.*, (1998), submitted.
12. M. H. Yoo, T. Takasugi, S. Hanada and O. Izumi, *Mater. Trans. JIM*, **31** (1990), 435.
13. B. J. Brindley, D. J. H. Corderoy and R. W. K. Honeycombe, *Acta Metall.*, **10** (1962), 1043.
14. X. Hu, H. Margolin, X. Duan and S. Nourbakhsh, *Scripta Metall. Mater.*, **26** (1992), 1257.
15. Y. Estrin, L. P. Kubin and E. C. Aifantis, *Scripta Metall. Mater.*, **29** (1993), 1147.
16. M. H. Yoo, F. Appel, R. Wagner and H. Mecking, in *Deformation and Fracture of Ordered Intermetallic Materials III*, ed. W. O. Soboyejo, T. S. Srivatasan, and H. L. Fraser (Warrendale, PA: TMS, 1996), 3.
17. *Binary Alloys Phase Diagrams*, vol. 1, ed. T. B. Massalski (Metals Park, OH: ASM,

1986), 112.
18. I. L. F. Ray, R. C. Crawford and D. J. H. Cockayne, *Phil. Mag.*, **21** (1970), 1027.
19. R. C. Crawford and I. L. F. Ray, *Phil. Mag.*, **35** (1977), 549.
20. M. G. Mendiratta, S. K. Ehlers, D. K. Chatterjee and H. A. Lipsitt, *Metall. Trans. A*, **18A** (1987), 283.
21. H. J. Leamy, E. D. Gibson and F. X. Kayser, *Acta Metall.*, **15** (1967), 1827.
22. M. H. Yoo, M. Koeppe, C. Hartig, H. Mecking, W. Hermann and H. -G. Sockel, *Acta Mater.*, **45** (1997), 4323.
23. G. Dlubek, O. Brümmer. J. Yli-Kauppila and J. Johansson, *Phys. Stat. Sol. (b)*, **106** (1981), K83.
24. H. -E. Schaefer, R. Würschum, M. Sob, T. Zak, W. Z. Yu, W. Eckert and F. Banhart, *Phys. Rev. B*, **41** (1990), 11869.
25. ZS. Tokei, J. Bernardini, P. Gas and D. L. Beke, *Acta Metall.*, **45** (1997), 541.
26. J. Wolff, M. Franz, Th. Hehenkamp, *J. Radioanalytical Nucl. Chem.*, **210** (1996), 591.
27. J. Wolff, M. Franz, A. Broska, B. Köhler and Th. Hehenkamp, *4th Int. Conf. on High Temp. Intermetallics*, (1997), in print.
28. R. Würschum, C. Grupp and H. -E. Schaefer, *Phys. Rev. Lett.*, **75** (1995), 97.
29. J. P. Rivière and J. Grilhé, *Phys. Stat. Sol. (a)*, **25** (1974), 429.
30. J. P. Rivière and J. Grilhé, *Scripta Metall.*, **9** (1975), 967.
31. J. P. Rivière, H. Zonon and J. Grilhé, *Phys. Stat. Sol. (a)*, **16** (1973), 545.
32. J. P. Rivière and J. Grilhé, *Acta Metall.*, **20** (1972), 1275.
33. T. Haraguchi and M. Kogachi, in *Structural Intermetallics 1997*, ed. M. V. Nathal, R. Darolia, C. T. Liu, P. L. Martin, D. B. Miracle, R. Wagner and M. Yamaguchi (Warrendale, PA: TMS, 1997), 769.
34. C. L. Fu, Y. -Y. Ye, M. H. Yoo and K. M. Ho, *Phys. Rev. B*, **48** (1993), 6712.

Table 1. Vacancy properties in B2 FeAl

Al content [mol%]	H_V^F [eV]	S_V^F	H_V^M [eV]	S_V^M	H_{2V}^B [eV]	S_{2V}^B	$H_{V\text{-}C}^B$ [eV]	Ref.
19.9			1.15					23
23.7	1.18	$5\,k_B$	1.4 - 1.6	($1\,k_B$)	0.6	($1\,k_B$)		24
24.4			1.31					23
25			1.2 (B2)					25
25	0.92		0.5					26
31	0.96							27
35	1.01							27
37	1.02							27
37	1.04	$6.5\,k_B$	1.7	($1\,k_B$)				28
38.5	0.94		1.57					29, 30
(38.5 - 47			$1.20 + 0.615S^2$	(S : long-range order parameter)				29)
39	0.98	$5.7\,k_B$	1.7	($1\,k_B$)				28
39	0.89	$4.2\,k_B$			≈ 0.5	($1\,k_B$)		28
40	0.91		1.61				0.15 - 0.23	30, 31, 32
40	0.98		1.2					27
43	1.42							27
44	0.83		1.67					29, 30
47	0.77		1.75					29, 30
47	0.86							33
48	1.38							27
48	0.6							33
49	0.44							33
50	0.5							33
50	0.97				0.57			34
50	0.52							8
51	0.41							33

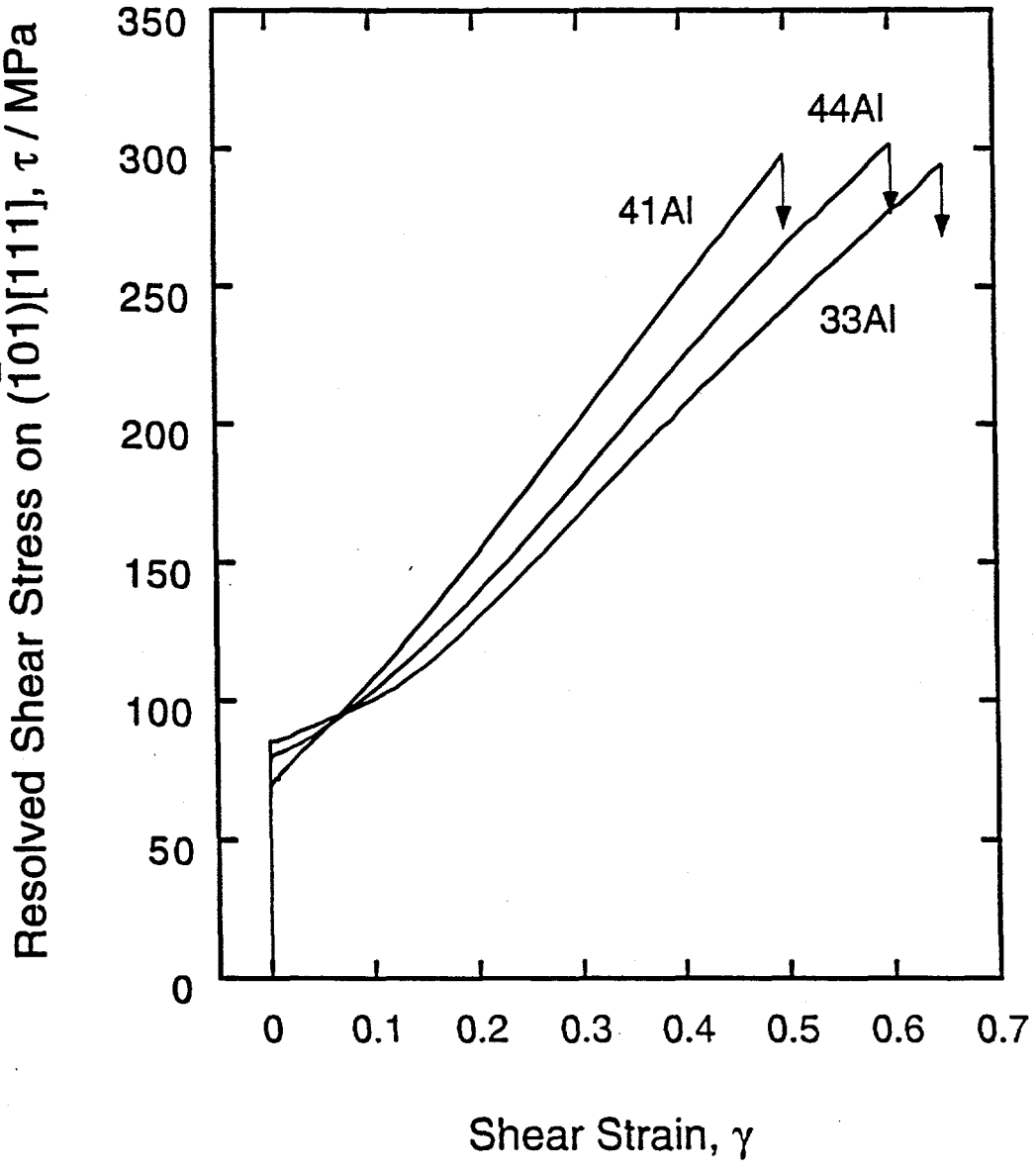

Fig. 1. Resolved shear stress-strain curves of as-homogenized Fe-33, 41 and 44mol.%Al single crystals.

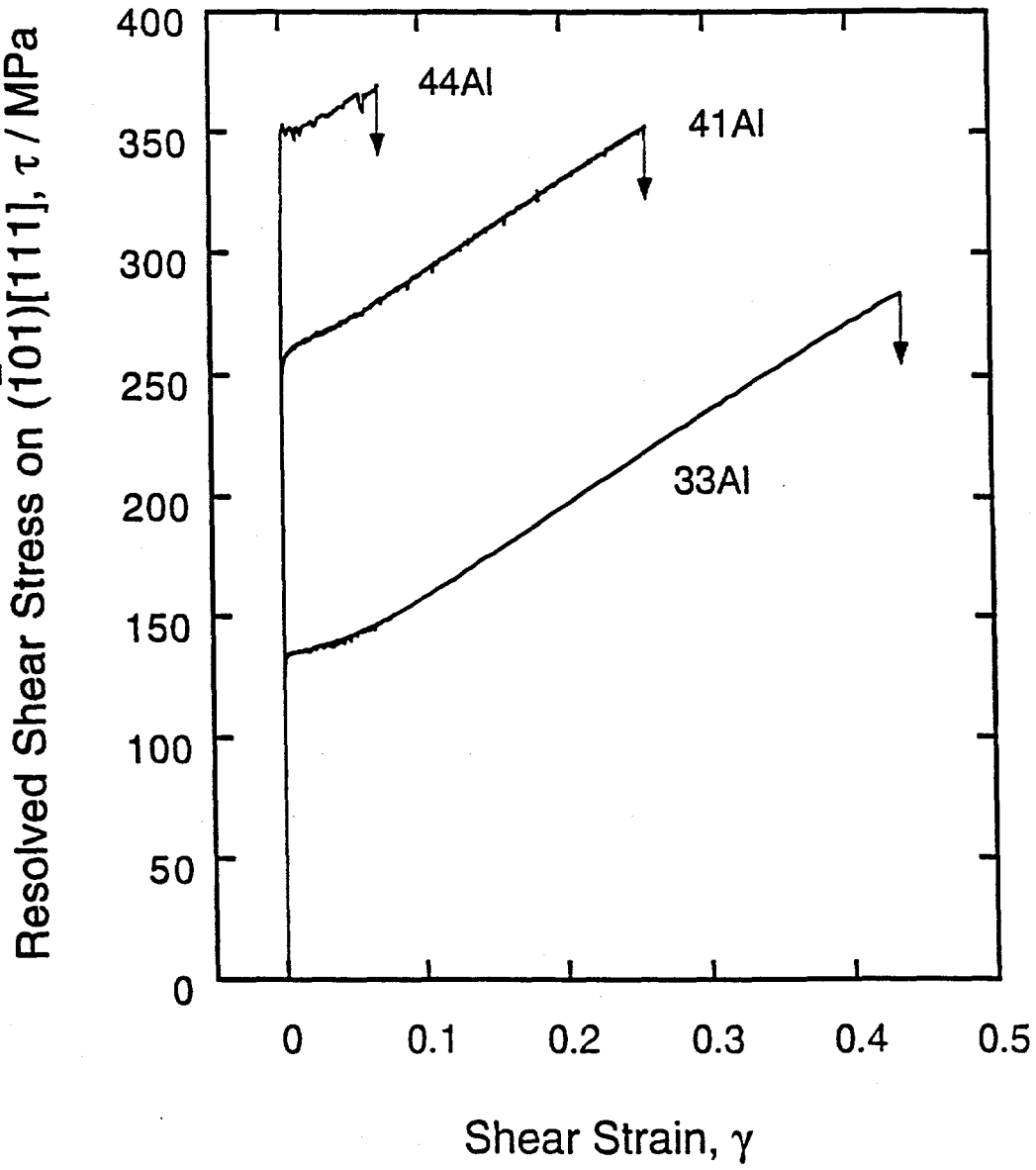

Fig. 2. Resolved shear stress-strain curves of fast-cooled Fe-33, 41 and 44mol.%Al single crystals.

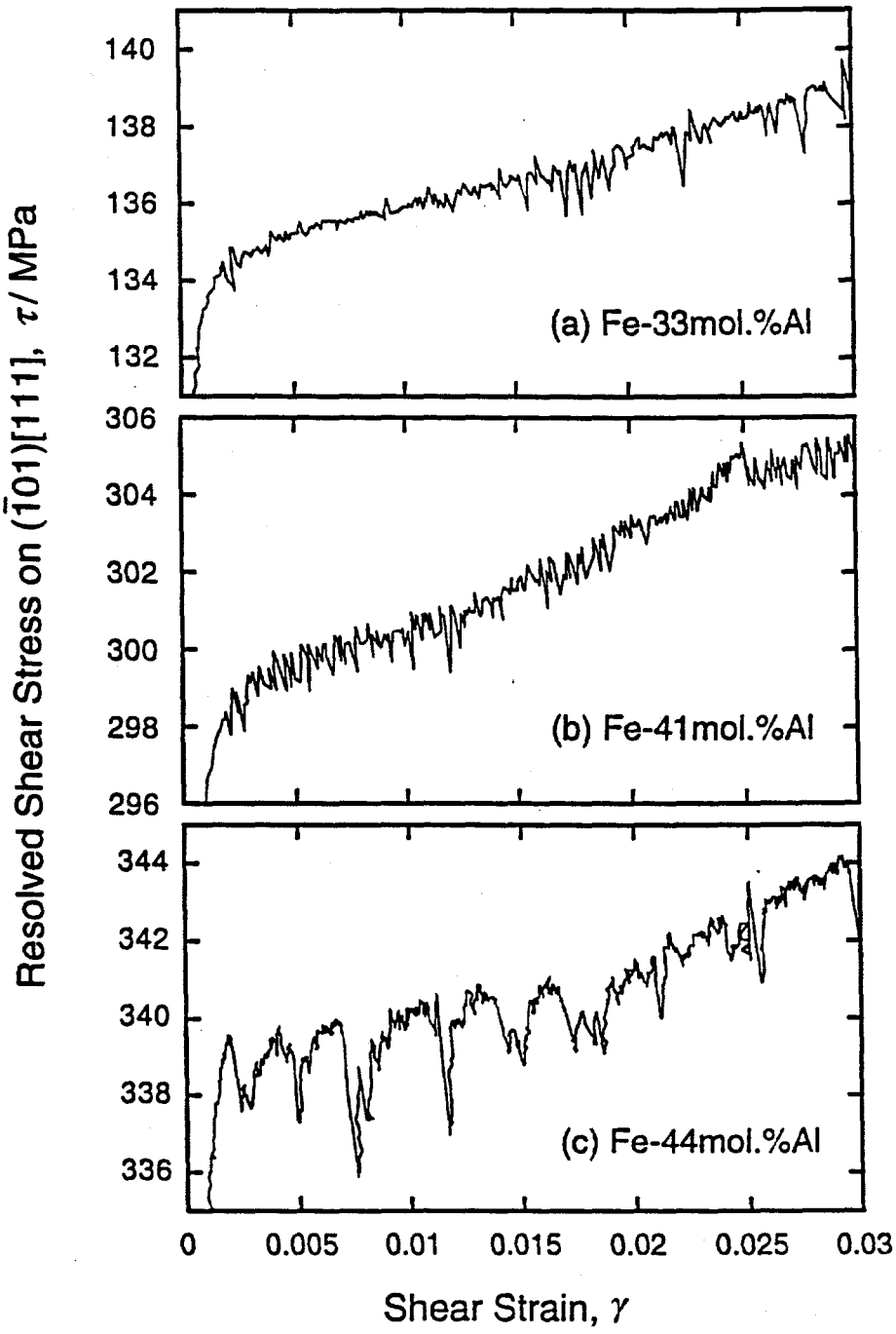

Fig. 3. Serrated flow of fast-cooled tensile specimens. (a) Fe-33mol.%Al. (b) Fe-41mol.%Al. (c) Fe-44mol.Al.

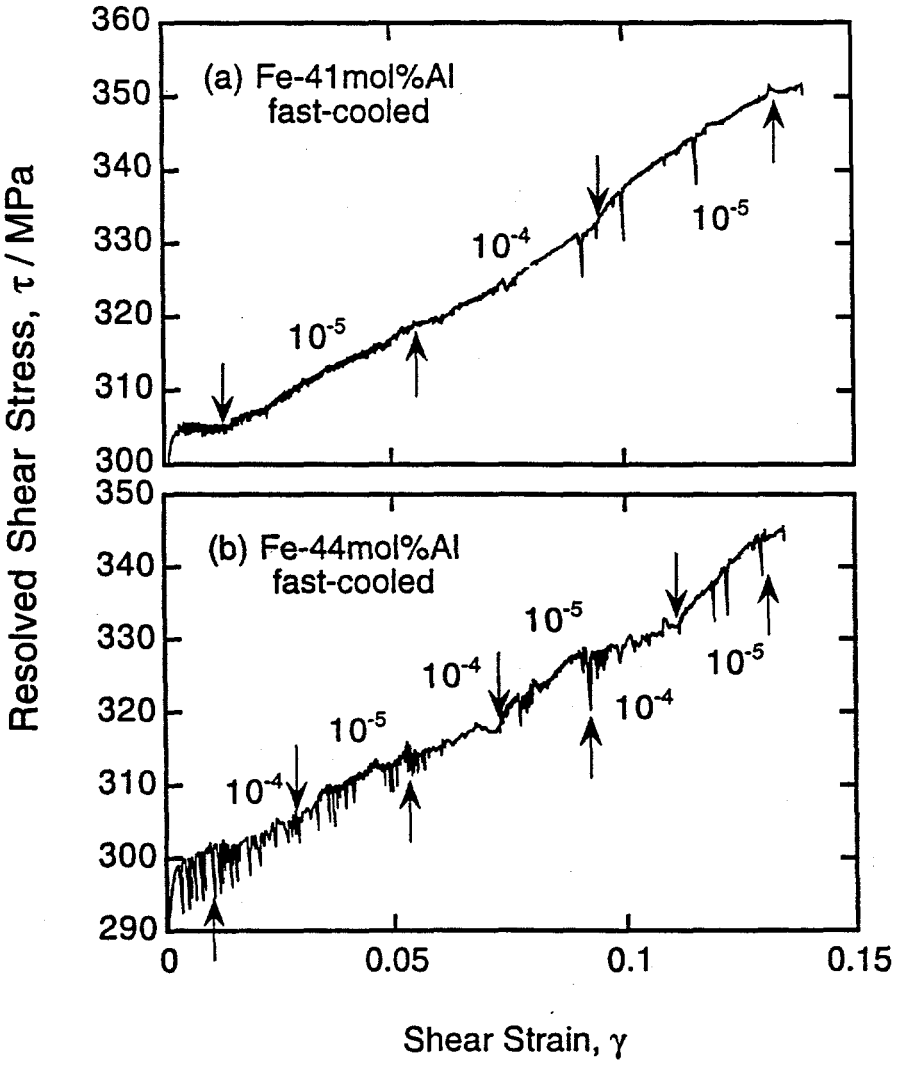

Fig. 4. Highly magnified resolved shear stress-strain curves of fast-cooled (a) Fe-41mol.%Al and (b) Fe-44mol.%Al during strain-rate change tests.

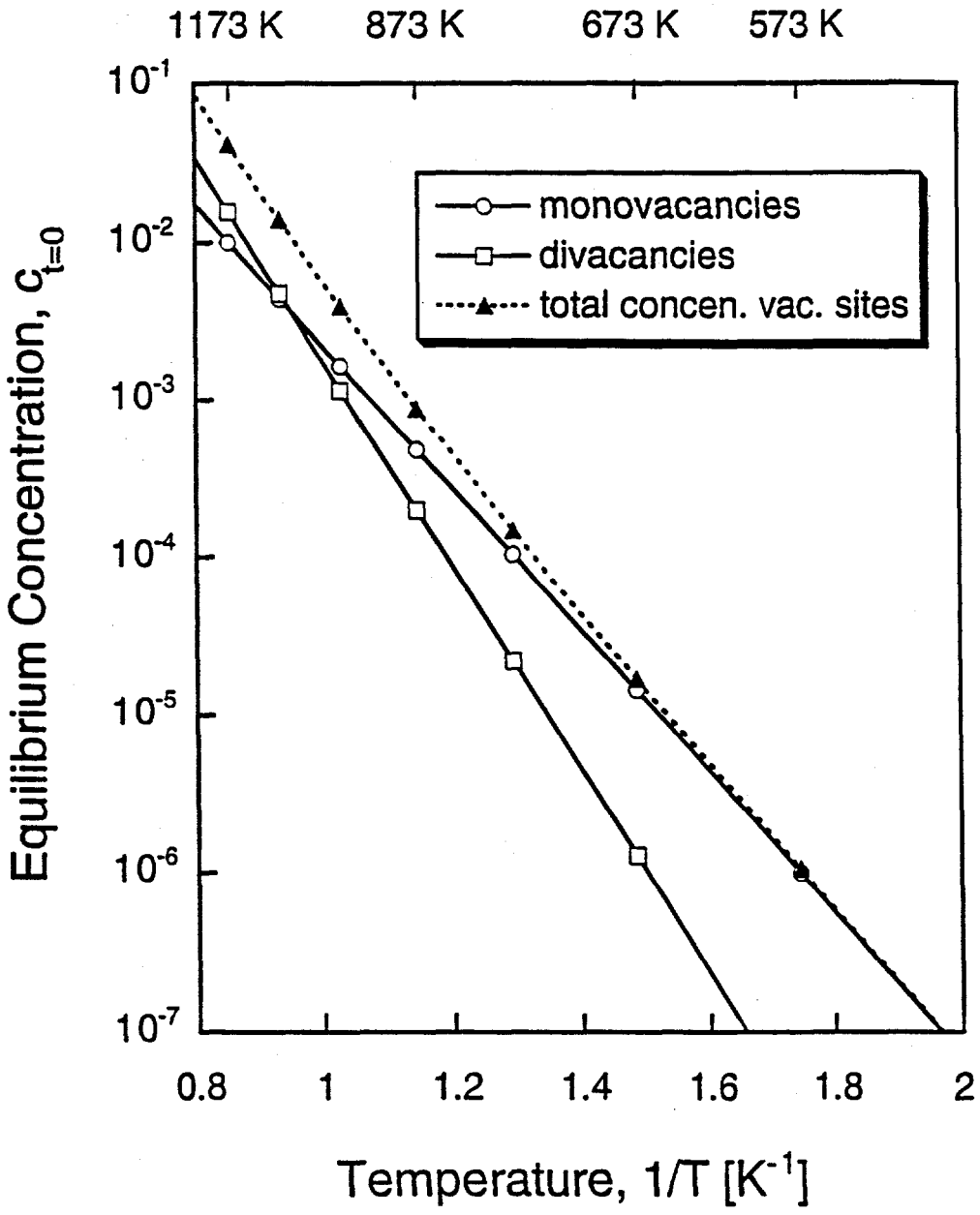

Fig. 5. Vacancy and divacancy concentrations in Fe-39Al as a function of temperature.